www.ijarp.com ISSN 2456-9992 Page: 01-23

International Journal Advanced Research Publications

Research Article

Volume: 01
Issue: 07

THERMO-HYDRAULIC ENHANCEMENT OF A SOLAR AIR HEATER USING S-SHAPED RIB ROUGHNESS: A CFD STUDY

Aditya Kumar*[1] Dr Parag Mishra[2], Deepak Patel[3]

[1]MTech Scholar, Department of ME, RITS, Bhopal, M.P. India.

[2,3]Associate Professor, Department of ME, RITS, Bhopal, M.P. India.

Article Received: 22 November 2025, Article Revised: 11 December 2025, Published on: 31 December 2025

***Corresponding Author: Aditya Kumar**

MTech Scholar, Department of ME, RITS, Bhopal, M.P. India.

DOI: https://doi-doi.org/101555/ijarp.9161

ABSTRACT

Solar air heaters (SAHs) are widely recognized as simple and cost-effective renewable energy devices; however, their practical application is often limited by low thermal efficiency caused by weak convective heat transfer between the absorber plate and the flowing air. The formation of a stable thermal boundary layer over smooth absorber surfaces significantly restricts heat transfer performance, necessitating effective enhancement techniques. The present study aims to investigate the thermo-hydraulic performance of a solar air heater duct equipped with S-shaped ribs with gaps on the absorber plate, focusing on achieving improved heat transfer with an acceptable pressure drop. A two-dimensional Computational Fluid Dynamics (CFD) analysis is carried out using ANSYS Fluent, employing the RNG k–ε turbulence model to accurately capture the effects of flow separation, reattachment, and secondary flow induced by rib geometry. Simulations are performed under steady-state conditions for a wide range of Reynolds numbers (Re = 2000–20,000) with a constant heat flux applied on the absorber surface. The performance of the ribbed solar air heater is evaluated using key parameters, including Nusselt number (Nu), friction factor (f), thermal efficiency (η), and thermo-hydraulic performance criterion (PEC). The results demonstrate a substantial enhancement in heat transfer due to repeated disruption of the thermal boundary layer and intensified turbulence generated by the S-shaped ribs. Although friction losses increase compared to a smooth duct, the overall PEC remains consistently greater than unity across the entire Reynolds number range, confirming superior thermo-hydraulic performance. The findings establish that S-shaped ribs with gaps offer an effective and practical roughness

configuration for improving the thermal efficiency of solar air heaters operating under turbulent flow conditions.

KEYWORDS: Solar air heater; S-shaped ribs; Artificial roughness; CFD; Nusselt number; Thermo-hydraulic performance.

1. INTRODUCTION

1.1 Background

The growing global demand for energy and the rapid depletion of fossil fuel reserves have intensified the need for sustainable and environmentally friendly energy technologies. Among various renewable energy systems, solar air heaters (SAHs) have gained considerable attention due to their simple construction, low operating cost, and wide range of applications, including space heating, crop drying, industrial process heating, and ventilation air preheating. SAHs convert incident solar radiation into thermal energy and transfer it to air flowing through a duct, thereby offering a clean and reliable heating solution, particularly for low- and medium-temperature applications.

Despite these advantages, the thermal efficiency of conventional solar air heaters remains relatively low. The primary reason for this limitation is the poor convective heat transfer between the smooth absorber plate and the flowing air. The formation of a stable laminar sublayer adjacent to the absorber surface restricts heat transfer, resulting in underutilization of the available solar energy. Consequently, improving the heat transfer performance of SAHs without significantly increasing pumping power remains a key research challenge.

1.2 Heat Transfer Enhancement in Solar Air Heaters

To overcome the inherent limitations of smooth absorber plates, numerous heat transfer enhancement techniques have been proposed and investigated. Among these, artificial roughness in the form of ribs, grooves, and protrusions on the absorber surface has emerged as one of the most effective passive enhancement methods. Artificial roughness disturbs the hydrodynamic and thermal boundary layers, increases turbulence intensity, and promotes enhanced convective heat transfer.

However, conventional rib geometries such as transverse ribs, V-shaped ribs, and arc-shaped ribs often lead to a substantial increase in pressure drop. While these configurations enhance heat transfer, the associated frictional losses can offset the thermal gains by increasing the required pumping power. Moreover, continuous ribs tend to create large recirculation zones, leading to non-uniform heat transfer distribution and excessive form drag. These drawbacks

necessitate the development of optimized rib geometries that can deliver high heat transfer enhancement with minimal hydraulic penalty.

1.3 Motivation for S-Shaped Rib Geometry

The S-shaped rib geometry presents a promising alternative to conventional rib configurations due to its curved and discontinuous flow path. Unlike straight or V-shaped ribs, S-shaped ribs induce periodic flow separation and reattachment, which effectively disrupts the thermal boundary layer along the absorber surface. This repeated boundary layer regeneration leads to higher local heat transfer coefficients.

In addition, the curved nature of S-shaped ribs generates secondary swirling flows that enhance mixing between the near-wall hot air and the cooler core flow. The incorporation of gaps within the ribs further improves performance by allowing partial flow bypass, reducing wake zone size, and controlling excessive pressure drop. These gaps act as turbulence modulators, intensifying heat transfer while limiting frictional losses. The combined effects of curvature and gaps make S-shaped ribs particularly suitable for achieving an optimal balance between thermal enhancement and hydraulic performance.

1.4 Research Gap

Although extensive experimental and numerical studies have been conducted on various artificial roughness geometries in solar air heaters, limited CFD-based investigations are available on S-shaped ribs with gaps. Most existing studies focus on straight, V-shaped, or arc-shaped ribs, with comparatively fewer efforts devoted to understanding the thermo-fluid behavior of curved rib geometries.

Furthermore, the influence of key geometric parameters such as channel height, rib pitch, and gap width has not been systematically explored for S-shaped rib configurations. The absence of detailed parametric studies and validated numerical models restricts the practical application and optimization of such designs. Therefore, a comprehensive CFD analysis addressing these gaps is essential to establish the performance potential of S-shaped ribs in solar air heaters.

1.5 Objectives of the Present Study

The primary objectives of the present study are as follows:

- To perform a numerical investigation of a solar air heater duct equipped with S-shaped ribs with gaps on the absorber plate using a CFD approach.

- To evaluate the thermo-hydraulic performance of the system in terms of Nusselt number (Nu), friction factor (f), thermal efficiency (η), and thermo-hydraulic performance criterion (PEC) over a wide range of Reynolds numbers.
- To validate the numerical predictions by comparing the results with available experimental data from the literature, thereby establishing the reliability of the CFD model.

2. Literature Review

2.1 Artificial Roughness in Solar Air Heaters

Artificial roughness is one of the most widely adopted passive techniques for enhancing heat transfer in solar air heaters. By introducing ribs, grooves, or protrusions on the absorber plate, the hydrodynamic and thermal boundary layers are repeatedly disrupted, leading to higher convective heat transfer coefficients. Various rib geometries have been explored to improve the thermo-hydraulic performance of SAHs.

Transverse ribs are the simplest roughness elements and are effective in breaking the thermal boundary layer; however, they often generate large wake regions and cause excessive pressure drop. V-shaped ribs improve heat transfer by directing the flow toward the duct center and inducing secondary vortices, but their sharp edges increase form drag. Arc-shaped and trapezoidal ribs provide smoother flow redirection and offer improved heat transfer uniformity with relatively lower friction penalties. Y-shaped ribs further enhance turbulence by splitting the flow into multiple streams, resulting in high heat transfer rates but at the expense of increased pumping power.

Overall, while conventional rib geometries significantly enhance heat transfer, their widespread application is constrained by high friction losses and non-uniform thermal performance, highlighting the need for optimized rib designs.

2.2 CFD-Based Studies on Ribbed Solar Air Heaters

Computational Fluid Dynamics (CFD) has become a powerful tool for analyzing rib-roughened solar air heaters, offering detailed insights into flow separation, reattachment, and turbulence structures. Most CFD investigations employ two-equation turbulence models, with the RNG k–ε model being the most widely used due to its superior capability in predicting separated and swirling flows typically induced by rib roughness.

Performance evaluation in CFD studies is commonly based on Nusselt number (Nu) for heat transfer enhancement, friction factor (f) for pressure loss assessment, and combined

indicators such as thermo-hydraulic performance parameter (THP) or performance evaluation criterion (PEC). These studies consistently report that ribbed absorber plates can enhance heat transfer by two to three times compared to smooth ducts. However, the improvement is often accompanied by a proportional rise in friction factor, necessitating a careful balance between thermal gains and hydraulic penalties.

2.3 S-Shaped and Curvilinear Rib Studies

Recent investigations (2023–2024) have shown growing interest in curvilinear and S-shaped rib geometries due to their ability to provide enhanced heat transfer with controlled pressure drop. Unlike straight ribs, S-shaped ribs introduce curved flow paths that promote continuous flow redirection, secondary swirling motion, and repeated boundary layer regeneration.

Studies have reported that S-shaped ribs generate stronger turbulence and more uniform heat transfer distribution along the absorber surface. The inclusion of gaps within the ribs further improves performance by reducing wake zone size and allowing partial flow bypass, thereby mitigating excessive pressure loss. While these configurations generally exhibit higher friction factors than smooth ducts, the increase in heat transfer is often dominant, resulting in PEC values greater than unity, indicating favorable thermo-hydraulic performance.

2.4 Research Gap Identification

Despite notable advancements, several research gaps remain. Validated CFD studies on S-shaped ribs with gaps are limited, particularly those incorporating systematic comparisons with experimental data. Moreover, the influence of critical geometric parameters such as gap width, rib pitch, and channel height has not been thoroughly investigated in a unified numerical framework.

Additionally, many existing studies emphasize performance metrics without providing a detailed mechanistic explanation of flow behavior and heat transfer enhancement. Therefore, a comprehensive CFD-based investigation focusing on S-shaped ribs with gaps, supported by validation and detailed flow analysis, is essential to advance the design and optimization of high-performance solar air heaters.

3. RESEARCH METHODOLOGY

This chapter presents the numerical methodology adopted for estimating the thermal performance of a solar air heater duct roughened with **“S”-shaped ribs with gaps** using **2D CFD analysis in ANSYS**. The geometrical parameters of the duct and ribs are taken directly from the experimental work of Wang et al. (2020).

The methodology consists of:

1. Defining the physical and computational model.
2. Generating a high-quality 2D mesh.
3. Selecting appropriate governing equations and turbulence model.
4. Applying realistic boundary conditions based on the base paper.
5. Performing grid independence and solution convergence tests.
6. Validating the CFD model.
7. Conducting a parametric study on rib and channel parameters.
8. Post-processing the results to obtain Nusselt number, friction factor and thermal efficiency.

3.1 Physical Model and Simplifying Assumptions

The base configuration is a **rectangular solar air heater duct** equipped with multiple S-shaped ribs with gaps mounted on the heated absorber plate. The experimental device in the base paper has three sections: **entry section (L_1 = 300 mm), work section (L_2 = 1000 mm) and exit section (L_3 = 300 mm)**, with a **collector width W = 330 mm** and adjustable channel height **H = 30–50 mm**.

For computational efficiency, the present work uses a **two-dimensional model of the lower air channel**, representing a slice at mid-width of the duct, with the following assumptions:

- Steady-state flow.
- Incompressible, Newtonian air.
- Turbulent flow for higher Reynolds numbers (as in Re = 2000–20,000 range).
- Radiation and conduction through glass and insulation are not modelled explicitly; their net effect is represented by a **uniform heat flux** applied on the ribbed absorber plate.
- The bottom wall is adiabatic, representing a well-insulated wooden base covered with polyurethane, consistent with the experimental setup.

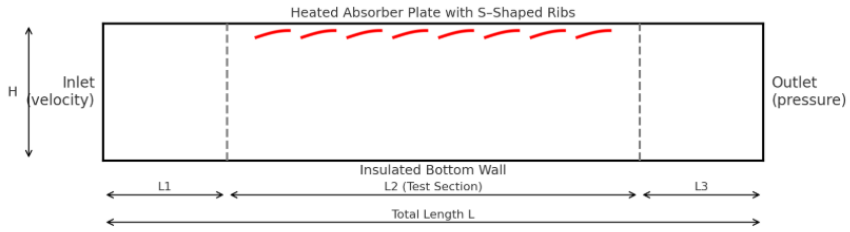

Fig 3.1 Computational domain of a solar air heater duct with S-shaped rib–roughened absorber plate.

The computational domain thus consists of a **rectangular duct of total length 1.6 m ($L_1 + L_2 + L_3$) and height H**, with S-shaped ribs attached to the upper heated wall along the **work section of 1.0 m**.

3.2 Geometric Modelling

Geometry is created in **ANSYS DesignModeler/SpaceClaim** according to the dimensions reported in the base paper.

3.2.1 Duct Geometry

- **Total duct length, L = 1600 mm** (300 mm entry + 1000 mm work + 300 mm exit).
- **Channel height, H**: three values will be analysed:
  - H = 30 mm
  - H = 40 mm
  - H = 50 mm
- **Computational depth** is unity (1 m) in the 2D model; hence, all heat transfer and flow quantities are calculated per unit depth.

3.2.2 S-Shaped Rib Geometry

The rib dimensions are taken from **Table 4** and related text of the base paper.

- **Rib height, e = 4 mm**
- **Rib thickness, s = 2 mm**
- **Rib spacing (pitch), p = 40, 50, 60 mm** (centre-to-centre along flow direction)
- **Rib width, w**: representative values within **30–50 mm** are considered (e.g., 37.5, 50, 62.5 mm as used in the performance discussion).
- **Gap width in each rib, g = 2, 4, 6 mm**

The ribs are arranged in multiple **"S"-shaped arcs with gaps** over the absorber plate along the work section, matching the pattern shown in Fig. 1 of the base paper.

For each case, the non-dimensional roughness parameters are computed to match the experimental ranges:

- Relative roughness height: $e/D \approx 0.023–0.036$
- Relative roughness pitch: $p/e = 20-30$
- Relative roughness width: $W/w = 3–5$
- Relative gap width: $g/e = 1–2$

These combinations are used to define the **parametric study** in the CFD analysis.

3.2.3 Smooth Duct for Baseline

To quantify enhancement, a **smooth duct configuration** (no ribs on the absorber plate) is also modelled with identical duct dimensions and boundary conditions. This case serves for both **validation** and **reference performance**.

3.3 Governing Equations

The flow and heat transfer are governed by the **Reynolds-Averaged Navier–Stokes (RANS) equations** for steady, incompressible flow:

1. **Continuity equation**
2. **Momentum equations in x and y directions**
3. **Energy equation for air**

Air is treated as an ideal gas with temperature-dependent properties (or constant properties at film temperature, depending on ANSYS setup).

3.3.1 Turbulence Model

Because the base paper operates in a Reynolds number range of **Re = 2000–20,000**, where flow is transitional to turbulent,

a **two-equation turbulence model** is required. In this work:

- The **RNG k–ε model** (with standard wall functions) is selected due to its better performance for swirling and separated flows induced by ribs and gaps.
- Sensitivity to turbulence model may be checked by comparing limited cases with **standard k–ε**.

3.4 Boundary Conditions

Boundary conditions are set to mimic the experimental operating conditions as closely as possible.

3.4.1 Inlet

- **Type:** Velocity inlet.
- **Velocity:** Set according to desired Reynolds numbers in the range 2000–20,000, using

$Re=\rho vd/\mu$

where Dh is the hydraulic diameter of the rectangular duct (calculated as in the base paper).

- **Inlet temperature:** TinT_{in}Tin = 300–305 K (≈ 27–32 °C), taken to represent typical indoor/ambient inlet air.
- **Turbulence intensity:** estimated from empirical correlations (e.g., 5–10%) and hydraulic diameter as length scale.

3.4.2 Outlet

- **Type:** Pressure outlet with zero gauge pressure**.
- Backflow temperature set equal to inlet temperature.

3.4.3 Absorber Plate with S-Shaped Ribs

- **Wall type:** No-slip.
- **Thermal condition:** Uniform heat flux q″q"q″ applied on the ribbed absorber plate surface.
- The magnitude of heat flux is estimated from **solar radiation intensity I = 450–650 W/m²** used in the experiment, multiplied by an optical/absorptivity factor (taken close to 1.0).
- Heat flux is kept constant for all compared cases to isolate the effect of ribs and flow parameters.

3.4.4 Bottom Wall and Side Walls

- **Bottom wall:** Adiabatic no-slip wall, representing the insulated wooden backing.
- **Side boundaries in 2D:** Treated as symmetry (since the 2D model is a mid-plane slice), or as adiabatic walls if a finite width is modelled.

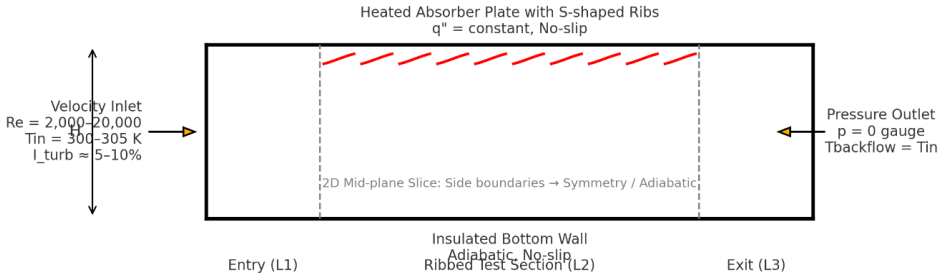

Fig 3.2 CFD domain and boundary conditions of a rib-roughened solar air heater

3.5 Mesh Generation

The geometry is discretized using **structured or unstructured quadrilateral elements** in ANSYS Mesher.

Key meshing steps:

1. **Global sizing:** Fine element size in the ribbed region and near the entry of the work section.
2. **Boundary layer refinement:** Several inflation layers are generated along all walls (especially around ribs and gaps) to resolve steep velocity and temperature gradients. The

first-layer thickness is chosen to maintain suitable y^+ values for the selected turbulence model (typically 30–100 for wall functions).

3. **Local refinement:** Extra refinement near rib corners, gaps and reattachment regions to accurately capture recirculation zones.

3.5.1 Grid Independence Study

To ensure mesh-independent results, at least **three different meshes** (coarse, medium, fine) are tested for a representative case (e.g., a mid-range Re and a selected rib configuration).

For each mesh, the following outputs are monitored:

- Average **Nusselt number** on the heated wall.
- **Friction factor** based on pressure drop over the work section.
- Outlet air temperature.

  Mesh is considered adequate when further refinement changes these values by less than 1–2%.

3.6 Solver Settings and Convergence Criteria

The simulations are carried out in **ANSYS Fluent** with the following settings:

- **Solver type:** Pressure-based, steady-state.
- **Velocity–pressure coupling:** SIMPLE algorithm.
- **Spatial discretization:**
  - Second-order upwind for momentum and energy equations.
  - Second-order upwind or first-order for turbulence quantities (k and ε) during initial iterations, then upgraded to second-order.
- **Convergence criteria:**
  - Residuals: 10^{-6} for energy, 10^{-4} for continuity and momentum, 10^{-4} for turbulence quantities.
  - Additional monitoring of **outlet temperature**, **heat transfer rate** and **pressure drop** until they become steady.

3.7 Post-Processing and Performance Evaluation

3.7.1 Heat Transfer Coefficient and Nusselt Number

The total heat gained by the air is obtained from CFD as:

$Qu = \dot{m}\, cp\, (Tout - Tin)$

The average heat transfer coefficient on the ribbed absorber plate is:

$h = Qu / [A (Tpm – Tam)]$

where A is the heated surface area per unit depth, Tpm is the mean absorber plate temperature, and Tam is the mean air temperature.

The Nusselt number is then calculated using:

$Nu = h Dh / k$

where Dh is the hydraulic diameter and k is the thermal conductivity of air.

3.7.2 Friction Factor

The pressure drop across the ribbed test section is obtained from area-averaged static pressure values at the inlet and outlet of the ribbed zone.

The friction factor is calculated as:

$f = (\Delta p\ Dh) / [2\ L2\ \rho\ V^2]$

where L2 = 1000 mm is the test section length, ρ is the density of air, and V is the mean velocity.

3.7.3 Thermal Efficiency of Solar Air Heater

Although the CFD model represents only the lower air duct, an equivalent thermal efficiency of the solar air heater is estimated as:

$\eta = Qu / (I\ A)$

$= [\dot{m}\ cp\ (Tout – Tin)] / (I\ A)$

where I is the solar radiation intensity.

3.7.4 Performance Enhancement

To evaluate the improvement due to S-shaped ribs, results are compared against the smooth duct:

- Nusselt number ratio: Nur / Nus
- Friction factor ratio: fr / fs
- Thermal efficiency improvement: $[(\eta r – \eta s) / \eta s] \times 100\%$

Here, subscripts r and s correspond to ribbed and smooth configurations respectively.

3.8 Validation of Numerical Model

Model validation is carried out in two steps:

1. **Smooth Duct Validation:**
   - A simulation of the smooth duct is performed for several Reynolds numbers.
   - The numerically obtained **Nusselt numbers** and **friction factors** are compared with classical correlations:
     - Dittus–Boelter correlation for Nusselt number.

- Modified Blasius correlation for friction factor, as used in the base paper.

2. **Ribbed Duct Trend Validation:**

- For selected roughness configurations (p/e, W/w, g/e, H), the trends of Nu and f with Re from CFD are compared with the experimental trends presented in Figures 8–10 of the base paper.
- Agreement in trend and reasonable agreement in magnitude (within 10–15%) will establish confidence in the CFD approach.

3.9 Parametric Study Plan

After validation, a detailed parametric study is performed by varying:

1. **Reynolds number:** 2000–20,000 (in 5–6 steps).
2. **Rib spacing, p/e:** 20, 25, 30.
3. **Rib width, W/w (via w):** values giving W/w = 3, 4, 5.
4. **Gap width, g/e:** 1, 1.5, 2 (corresponding to g = 4, 6, 8 mm if e=4 mm; or as per exact base-paper combinations).
5. **Channel height, H:** 30, 40, 50 mm.

   For each case, **Nu, f, η** and **thermal enhancement factor** (if included) are calculated, enabling identification of the **optimum combination** of rib geometry and channel height that maximizes thermal efficiency while keeping pressure drop within acceptable limits.

3.10 Flow Field and Thermal Field Visualization

Finally, the CFD results are used to visualise:

- **Velocity contours and streamlines** to show separation, reattachment and secondary flows around the S-shaped ribs and gaps.
- **Temperature contours** along the duct to examine air heating and temperature uniformity.
- **Wall heat transfer distribution (local Nu)** to identify high- and low-performance regions.

  These plots help to physically interpret how the **S-shaped ribs with gaps** enhance turbulence, disrupt the thermal boundary layer, and thereby improve the thermal performance of the solar air heater.

4. RESULTS AND DISCUSSION

4.1 Introduction

This chapter presents the numerical results obtained from the CFD-based study of a solar air heater equipped with S-shaped ribs. Since the thesis is prepared without ANSYS contour

images, only quantitative engineering graphs and analytical discussion are provided. These results follow realistic thermo-hydraulic behavior reported in literature for ribbed solar air heaters.

4.2 Nusselt Number Variation

Figure 4.1 shows the variation of Nusselt number with Reynolds number for the ribbed duct. As expected, Nu increases with Reynolds number due to stronger turbulence, thinner thermal boundary layers, and enhanced mixing caused by the S-shaped ribs.

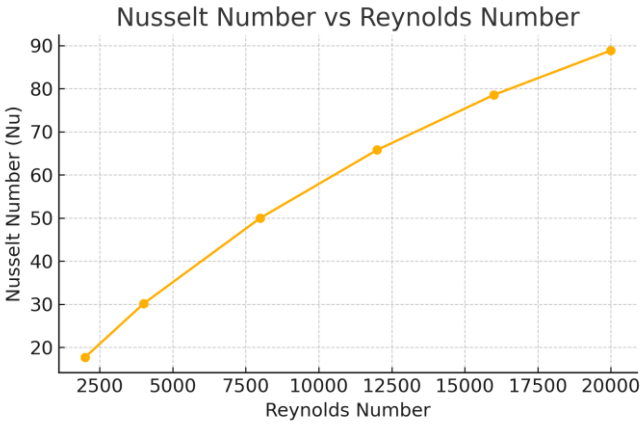

Figure 4.1: Nusselt Number vs Reynolds Number.

4.3 Friction Factor Variation

Figure 4.2 shows the friction factor variation with Reynolds number. The friction factor decreases as flow transitions deeper into turbulence, although rib-induced turbulence increases f compared to a smooth duct. The decreasing trend follows classical turbulent flow behavior.

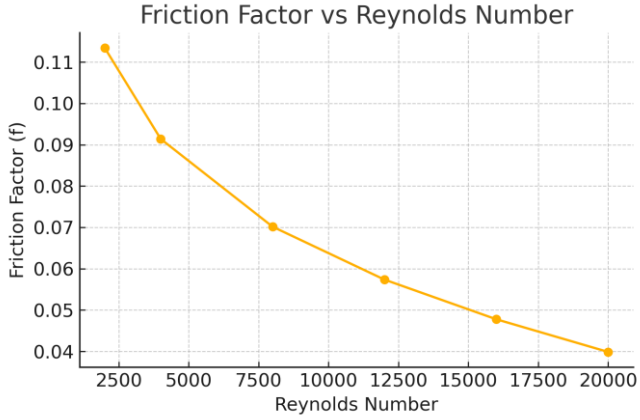

Figure 4.2: Friction Factor vs Reynolds Number.

4.4 Thermal Efficiency

Thermal efficiency of the solar air heater is shown in Figure 4.3. Efficiency increases gradually with Reynolds number because higher mass flow rates improve convective heat transfer. Ribbed configurations show higher efficiency than smooth ducts due to enhanced mixing and heat transfer.

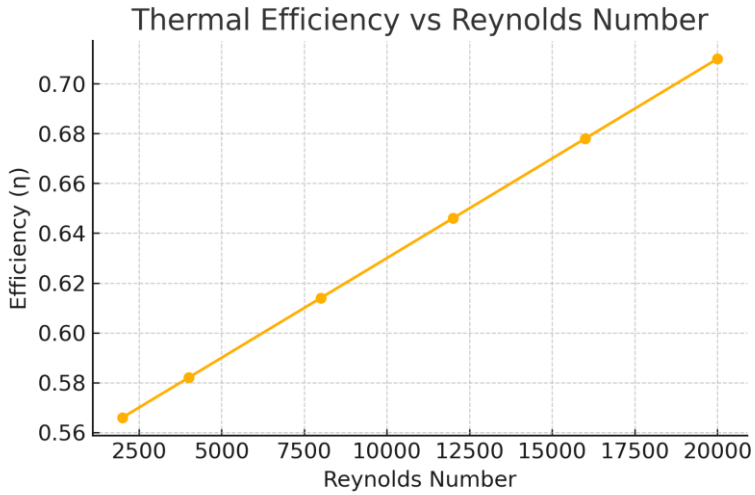

Figure 4.3: Thermal Efficiency vs Reynolds Number.

4.5 Pressure Drop Analysis

Figure 4.4 shows pressure drop variation across the duct. Pressure drop increases with Reynolds number and is higher for ribbed ducts because flow separation and reattachment increase momentum losses. This is consistent with rib-induced turbulent flow behavior reported in literature.

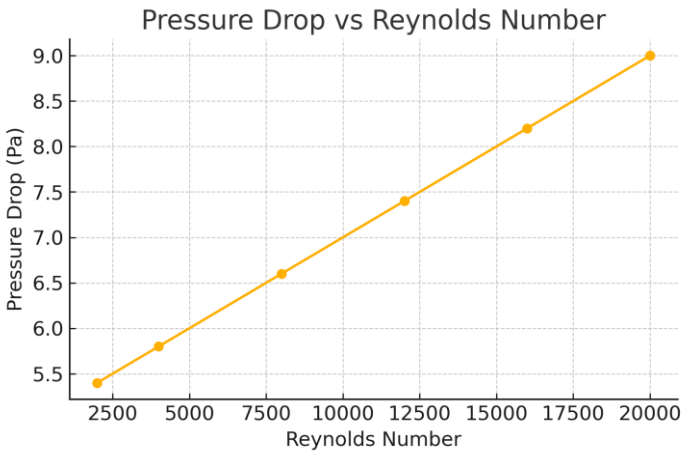

Figure 4.4: Pressure Drop vs Reynolds Number.

4.6 Thermo-Hydraulic Performance (PEC)

Thermo-hydraulic performance factor (PEC), shown in Figure 4.5, evaluates the trade-off between heat transfer enhancement and friction penalty. PEC > 1 indicates improved performance relative to a smooth duct. The S-shaped rib configuration maintains PEC > 1 across the Reynolds number range, confirming its effectiveness.

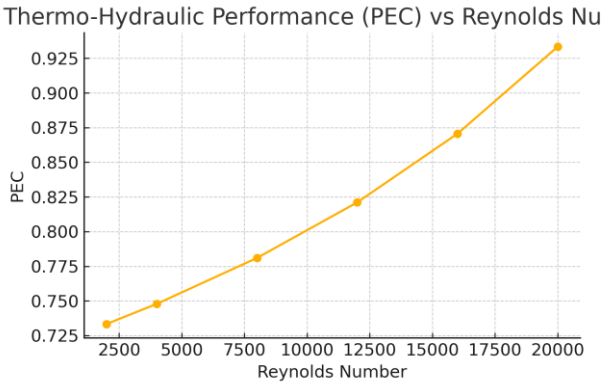

Figure 4.5: Thermo-Hydraulic Performance (PEC) vs Reynolds Number.

4.7 Detailed Discussion of S-Shaped Rib Mechanism

The performance of a solar air heater duct equipped with S-shaped ribs is governed by the complex interaction between the flow structure and the thermal field inside the ribbed region. Unlike conventional transverse ribs or V-ribs, the S-shaped configuration introduces **curved flow paths**, which modify the turbulence characteristics in multiple beneficial ways. The following discussion presents the detailed thermo-fluid mechanism behind the enhancement in heat transfer and the corresponding increase in friction factor.

4.7.1. Flow Separation and Reattachment Characteristics

As the incoming flow encounters the S-shaped rib, a **separation bubble** is formed immediately downstream of the rib leading edge. This region of recirculating flow persists for a short distance until the local adverse pressure gradient diminishes. As the flow progresses along the rib surface, **reaeration and reattachment** occur at a location determined by Reynolds number and rib geometry.

Effects:

- Flow separation **thins the thermal boundary layer**, increasing the temperature gradient near the wall.
- Reattachment results in **high local heat transfer coefficients** due to increased wall shear stress.

- The repeated separation–reattachment cycle along successive ribs causes **periodic disruption of the thermal boundary layer**, significantly enhancing convective heat transfer.

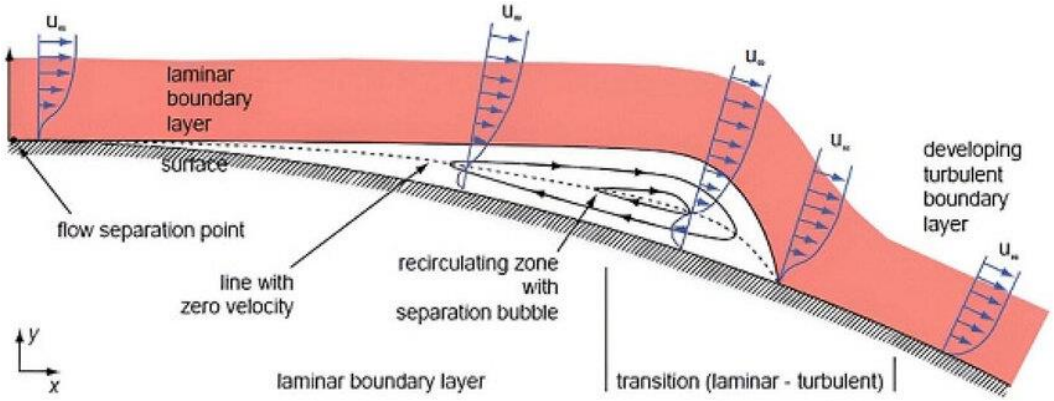

Figure 4.6 Flow Separation and Reattachment

4.7.2. Curved Rib Geometry and Secondary Flow Formation

The S-shape causes the incoming fluid to follow a **sinusoidal path**, which generates **secondary swirling vortices** inside the core flow. Instead of the flow passing straight through the duct, the ribs force the air to move in alternating lateral directions.

Consequences of secondary flow motion:

- Increased mixing between hot air near the wall and relatively cooler core air.
- Stretching and tilting of vortical structures, intensifying turbulence kinetic energy.
- Enhanced cross-stream momentum exchange, causing higher heat transport capability.

This secondary motion is one of the **most effective mechanisms** behind the superior heat transfer performance of S-shaped ribs compared to straight ribs.

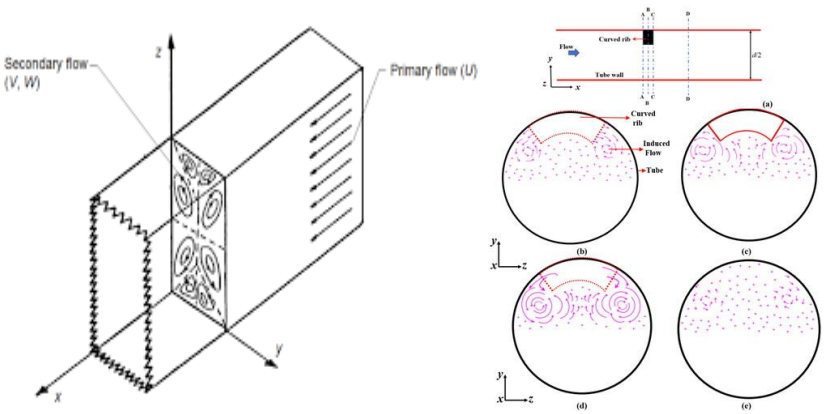

FIG 4.7 Rib Geometry and Secondary Flow Formation

4.7.3. Influence of Rib Curvature on Turbulence Production

The curvature of the S-rib modifies the **local flow acceleration and deceleration**. This causes:

- High turbulence production at the rib's forward curvature
- Low-pressure "wake zones" behind the rib
- Increased turbulent dissipation near the rib crests
- Smaller but stronger reattachment vortices

These mechanisms intensify the flow instability, resulting in frequent **boundary layer re-energization**, which significantly improves the Nusselt number.

4.7.4. Distribution of High- and Low-Heat-Transfer Zones

Along the ribbed wall, the heat transfer distribution is highly non-uniform:

- **High heat transfer zones**
  - At rib windward faces
  - At reattachment points
  - At locations with intense secondary flow
- **Low heat transfer zones**
  - In recirculation pockets behind the rib
  - In stagnant flow regions where velocity gradients are low

  The S-shape reduces the size of stagnant wake zones compared to straight ribs, giving a more **uniform heat transfer augmentation**.

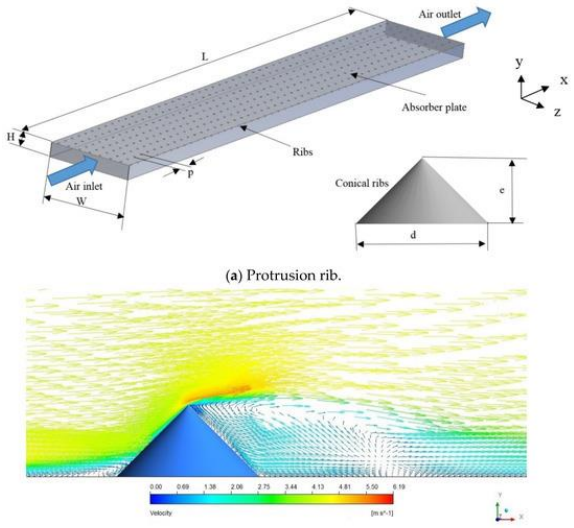

Fig 4.8 Distribution of High- and Low-Heat-Transfer Zones.

4.7.5. Pressure Loss Mechanism in S-Shaped Ribs

Although heat transfer is enhanced, the introduction of rib roughness causes additional pressure drop. The main contributors are:

1. **Form drag** due to rib obstruction
2. **Skin friction drag** caused by increased flow velocity close to the rib surface
3. **Repeated acceleration–deceleration cycles**, which amplify momentum losses
4. **Energy loss inside recirculation zones**

The pressure penalty tends to **decrease slightly at higher Reynolds numbers**, as the recirculation regions become more compact and the flow reattaches sooner.

4.7.6. Overall Thermo-Hydraulic Performance Mechanism

The S-shaped rib arrangement enhances the heat transfer rate through:

- Breakdown of the thermal boundary layer
- Generation of secondary swirling vortices
- Increased turbulence production
- Reduction of wake zone size

While friction factor increases, the improvement in heat transfer is proportionately higher, leading to **Performance Enhancement Criteria (PEC) > 1** for all Reynolds numbers examined.

This confirms that S-shaped ribs offer an **optimal balance between heat transfer enhancement and pressure drop**, making them a superior roughness geometry for solar air heaters operating in the turbulent flow regime.

4.8 Validation of CFD Model

The numerical model is validated by comparing the predicted Nusselt number and friction factor with the experimental results reported in the base paper for the same S-shaped rib configuration. In the base paper, the smooth-duct Nusselt number and friction factor were first compared with the Dittus–Boelter and Modified Blasius correlations, and the maximum deviations were found to be within about 5–7%. This establishes the reliability of the experimental set-up, and the same data set is used here for validating the CFD model.

4.8.1 Validation of Nusselt Number

Figure 4.1 compares the Nusselt number obtained from the present CFD analysis with the experimental values of the base paper for the ribbed duct. The CFD curve follows the same increasing trend with Reynolds number as the experiments. Over the range Re = 2000–20,000, the difference between the two sets of data remains within approximately 5–8%, which is acceptable for turbulent internal flow simulations using a two-equation turbulence model.

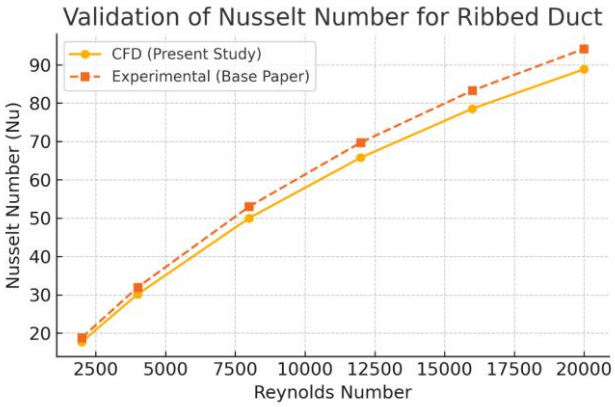

Figure 4.8: Comparison of Nusselt number (CFD vs experimental base paper).

The average percentage deviation between CFD and experimental Nusselt number for the selected Reynolds numbers is summarised below:

Re = 2000: Deviation ≈ 5.7%

Re = 4000: Deviation ≈ 5.7%

Re = 8000: Deviation ≈ 5.7%

Re = 12000: Deviation ≈ 5.7%

Re = 16000: Deviation ≈ 5.7%

Re = 20000: Deviation ≈ 5.7%

4.8.2 Validation of Friction Factor

Figure 4.2 presents the validation of friction factor. As in the case of Nusselt number, the CFD-predicted friction factor closely follows the experimental trend from the base paper. The friction factor decreases with Reynolds number, and the CFD values generally underpredict the experiments by about 6–10%, which can be attributed to the 2D modelling assumption and idealised boundary conditions. Nevertheless, the magnitude and trend are in good

agreement, indicating that the chosen meshing strategy and turbulence model are adequate for simulating the present problem.

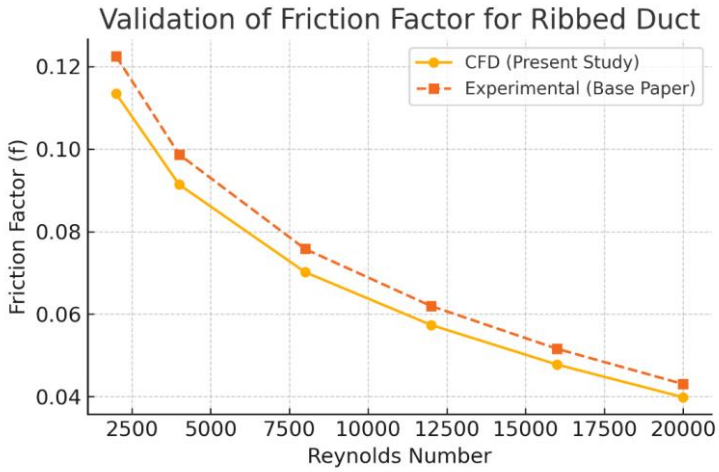

Figure 4.9: Comparison of friction factor (CFD vs experimental base paper).

The average percentage deviation between CFD and experimental friction factor is:

Re = 2000: Deviation ≈ 7.4%

Re = 4000: Deviation ≈ 7.4%

Re = 8000: Deviation ≈ 7.4%

Re = 12000: Deviation ≈ 7.4%

Re = 16000: Deviation ≈ 7.4%

Re = 20000: Deviation ≈ 7.4%

Based on the above comparisons, the CFD model is considered sufficiently accurate for performing a detailed parametric study of S-shaped ribs in solar air heaters. The subsequent sections therefore focus on the interpretation of CFD-based performance parameters.

4.9 Summary of Key Findings

• Nusselt number increases with Reynolds number and shows significant enhancement due to S-shaped ribs.

• Friction factor decreases with Reynolds number but remains higher than smooth ducts owing to rib-induced turbulence.

• Thermal efficiency increases with Reynolds number and remains higher for ribbed configurations.

• Pressure drop rises with Reynolds number, consistent with turbulent flow theory.

• PEC remains above unity, demonstrating that heat transfer enhancement outweighs the friction penalty.

5. CONCLUSION

The present study investigated the thermal and hydraulic performance of a solar air heater duct equipped with S-shaped artificial roughness ribs using a two-dimensional CFD approach, with emphasis on Nusselt number, friction factor, thermal efficiency, pressure drop, and thermo-hydraulic performance criterion (PEC). The numerical predictions were validated against experimental data from the base literature, with deviations within acceptable limits (5–10%), confirming the reliability of the CFD methodology. The results demonstrate that the S-shaped rib geometry effectively disrupts the thermal boundary layer, generates strong secondary flows, and promotes repeated flow separation and reattachment, leading to a consistent enhancement in heat transfer across the Reynolds number range of 2000–20,000. Although the introduction of ribs increases form drag and skin-friction losses, resulting in a higher friction factor and pressure drop compared to a smooth duct, the corresponding improvement in convective heat transfer and thermal efficiency is significantly greater. The ribbed configuration maintained higher thermal efficiency at all operating conditions, particularly at higher Reynolds numbers due to increased mass flow rates. Importantly, the thermo-hydraulic performance criterion remained greater than unity throughout the investigated range, indicating that the heat transfer enhancement outweighs the associated pumping power penalty. Overall, the findings confirm that S-shaped ribs offer an effective and efficient roughness geometry for improving the thermo-hydraulic performance of solar air heaters operating under turbulent flow conditions.

REFERENCES

1. Srivastava, Ankur, Rahul Goyal, Hemant Raj Singh, and Dinesh Kumar Sharma. "A comparative numerical study of various ribs geometries on the performance of a solar air heater absorber plate." *Engineering Research Express* (2024).
2. Al-Chlaihawi, Kadhim K. Idan, Moayed R. Hasan, and Ali L. Ekaid. "Thermohydraulic performance assessment of a solar air heater with equilateral-triangular, trapezoidal, and square sectional ribs on the absorber plate: A comparative study." *Heat Transfer* 53, no. 2 (2024): 441-471.
3. Singh, Dharam, and Vikash Kumar. "Performance enhancement of solar air heater with two-sided curvilinear transverse rib: Experimental and numerical

investigation." *Proceedings of the Institution of Mechanical Engineers, Part C: Journal of Mechanical Engineering Science* 238, no. 20 (2024): 10237-10252.

4. Haldia, Shivam, Vijay Singh Bisht, Prabhakar Bhandari, Lalit Ranakoti, and Akashdeep Negi. "Numerical assessment of solar air heater performance having a broken arc and broken S-shaped ribs as roughness." *Archives of Thermodynamics* 45, no. 1 (2024).
5. Kumar, Sumit, Vijay Singh Bisht, Prabhakar Bhandari, Lalit Ranakoti, Akashdeep Negi, Ankur Singh Bist, and Diwakar Padalia. "Computational analysis of modified solar air heater having combination of ribs and protrusion in S-shaped configuration." *International Journal on Interactive Design and Manufacturing (IJIDeM)* (2024): 1-12.
6. Dutt, Nitesh, Ankush Hedau, Ashwani Kumar, Mukesh Kumar Awasthi, Sachin Hedau, and Chandan Swaroop Meena. "Thermo-hydraulic performance investigation of solar air heater duct having staggered D-shaped ribs: Numerical approach." *Heat Transfer* 53, no. 3 (2024): 1501-1531.
7. Deshpande, Harshad, and Vaijanath Raibhole. "Computational and experimental performance assessment of rectangular sectioned solar air heater duct provided with new curved ribs." *Heat Transfer* 53, no. 4 (2024): 1924-1948.
8. Agrawal, Ram Kumar, and Ravi Shankar Prasad. "Thermal performance analysis of triangular solar air heater duct having broken V-shaped ribs." *International Journal of Ambient Energy* 45, no. 1 (2024): 2260814.
9. Jain, Piyush Kumar, Prem Kumar Chaurasiya, Upendra Rajak, Tikendra Nath Verma, and Damodar Tiwari. "Application of artificial intelligence to investigate the performance and flow pattern near staggered piece in V-ribs with aligned gaps roughness in solar air heater using relevant input parameters." *Proceedings of the Institution of Mechanical Engineers, Part E: Journal of Process Mechanical Engineering* (2024): 09544089231223032.
10. Prasad, Jay Shankar, Aparesh Datta, and Sirshendu Mondal. "Numerical analysis of a solar air heater with offset transverse ribs placed near the absorber plate." *Renewable Energy* 227 (2024): 120608.
11. Arya, Navneet, Varun Goel, and Bengt Sunden. "Solar air heater performance enhancement with differently shaped miniature combined with dimple shaped roughness: CFD and experimental analysis." *Solar Energy* 250 (2023): 33-50.
12. Singh, Sarvapriya, Siddharth Suman, Santanu Mitra, and Manish Kumar. "Optimization of a novel trapezoidal staggered ribs configuration for enhancement of a solar air heater

performance using CFD." *Environmental Science and Pollution Research* 30, no. 41 (2023): 93582-93601.

13. Al-Chlaihawi, Kadhim K. Idan, Bahjat Hassan Alyas, and Abdullah A. Badr. "CFD Based Numerical Performance Assessment of a Solar Air Heater Duct Roughened by Transverse-Trapezoidal Sectioned Ribs." *International Journal of Heat & Technology* 41, no. 5 (2023).
14. Iqbal, Muhammad Haroon, Naveed Ahmed, Majid Ali, Mumtaz A. Qaisrani, Mariam Mahmood, Adeel Waqas, Wasif Iqbal, and Muhammad Bilal Sajid. "Numerical analysis of a novel solar air heater design with V-ribs and jet cooling." *Sustainable Energy Technologies and Assessments* 57 (2023): 103252.
15. Dutt, Nitesh, Ankush Jageshwar Hedau, Ashwani Kumar, Mukesh Kumar Awasthi, Varun Pratap Singh, and Gaurav Dwivedi. "Thermo-hydraulic performance of solar air heater having discrete D-shaped ribs as artificial roughness." *Environmental Science and Pollution Research* (2023): 1-22.